Journal of Applied Physics

Self-heating of cryogenic high electron-mobility transistor amplifiers and the limits of microwave noise performance

Cite as: J. Appl. Phys. **132**, 084501 (2022); https://doi.org/10.1063/5.0103156
Submitted: 14 June 2022 • Accepted: 26 July 2022 • Published Online: 22 August 2022

Anthony J. Ardizzi, Alexander Y. Choi, Bekari Gabritchidze, et al.

AIP Publishing

Journal of Applied Physics ARTICLE scitation.org/journal/jap

Self-heating of cryogenic high electron-mobility transistor amplifiers and the limits of microwave noise performance

Cite as: J. Appl. Phys. **132**, 084501 (2022); doi: 10.1063/5.0103156
Submitted: 14 June 2022 · Accepted: 26 July 2022 ·
Published Online: 22 August 2022

Anthony J. Ardizzi,[1] Alexander Y. Choi,[1] Bekari Gabritchidze,[2,3] Jacob Kooi,[4] Kieran A. Cleary,[2] Anthony C. Readhead,[2] and Austin J. Minnich[1,a)]

AFFILIATIONS

[1]Division of Engineering and Applied Science, California Institute of Technology, Pasadena, California 91125, USA
[2]Division of Physics, Mathematics, and Astronomy, California Institute of Technology, Pasadena, California 91125, USA
[3]Department of Physics, University of Crete, GR-70 013 Heraklion, Greece
[4]Jet Propulsion Laboratory, California Institute of Technology, Pasadena, California 91109, USA

[a)]**Author to whom correspondence should be addressed:** aminnich@caltech.edu

ABSTRACT

The fundamental limits of the microwave noise performance of high electron-mobility transistors (HEMTs) are of scientific and practical interest for applications in radio astronomy and quantum computing. Self-heating at cryogenic temperatures has been reported to be a limiting mechanism for the noise, but cryogenic cooling strategies to mitigate it, for instance, using liquid cryogens, have not been evaluated. Here, we report microwave noise measurements of a packaged two-stage amplifier with GaAs metamorphic HEMTs immersed in normal and superfluid ^{4}He baths and in vacuum from 1.6 to 80 K. We find that these liquid cryogens are unable to mitigate the thermal noise associated with self-heating. Considering this finding, we examine the implications for the lower bounds of cryogenic noise performance in HEMTs. Our analysis supports the general design principle for cryogenic HEMTs of maximizing gain at the lowest possible power.

I. INTRODUCTION

Microwave low-noise amplifiers (LNAs) based on III–V semiconductor high electron mobility transistor (HEMT) technology[1,2] are a key component of high precision measurements across diverse fields in science and engineering, such as radio astronomy,[3,4] deep-space communication,[5] and quantum computing.[6–10] In these applications, LNAs serve as the first or second stage of amplification in the receiver chain, thereby making a decisive contribution to the noise floor of the entire measurement apparatus. Although marked improvements in noise performance have been achieved in recent decades,[5,11–17] the noise performance of HEMT LNAs remains a factor of 3–5 larger than the quantum limit.[4,18,19]

The noise behavior of HEMT amplifiers is typically interpreted using the Pospieszalski model.[20] In this model, noise generators are assigned to the gate resistance at the input and the drain conductance at the output, parameterized by noise temperatures T_g and T_d, respectively. The drain temperature T_d lacks an accepted physical origin, with several theories having been proposed,[21–24] and it is typically taken as a fitting parameter. The gate temperature T_g is assumed to be equal to the physical device temperature.[1,25] In this interpretation, cryogenic cooling leads to improvements in the noise figure of the HEMT, in part, by decreasing the gate temperature and hence its thermal noise.

The monotonic decrease in the noise figure with decreasing physical temperature has been observed to plateau below physical temperatures of 20–40 K (see Fig. 10 from Ref. 26, Fig. 1 from Ref. 27, and Fig. 2 from Ref. 28, for example). Recent numerical and experimental studies have attributed this plateau to heating of the gate caused by power dissipated in the active channel, referred to as self-heating.[27,29] In more detail, optimal low-noise performance at cryogenic temperatures requires power dissipation on the order of milliwatts. At these temperatures, the observed thermal resistance from Schottky thermometry is consistent with that expected of phonon radiation for which the thermal resistance varies as T^{-3}.[30]

Consequently, at physical temperatures $\lesssim$20 K, the rapid increase in thermal resistance with decreasing temperature leads to a plateau in the gate temperature, which produces a corresponding plateau in the noise figure.

Mitigating the effect of self-heating by enhancing heat dissipation is desirable. However, cryogenic thermal management of the gate in modern devices with sub-micrometer gate lengths and a buried gate structure is challenging. Existing on-chip cooling methods[31] must be evaluated for their capability to provide cooling while avoiding detrimental impact on device noise performance. An alternate approach that does not require any device modifications is to submerge the heated surface in superfluid ^{4}He, a quantum fluid with the highest known thermal conductivity.[32] Such an approach is routinely used for cryogenic thermal management of superconducting magnets[33] and is actively employed in high-energy physics experiments.[34–36] However, the effectiveness of liquid cryogens to mitigate self-heating in HEMTs has not been experimentally evaluated.

Here, we present noise measurements of a packaged two-stage amplifier with GaAs metamorphic HEMTs immersed in normal (He I) and superfluid (He II) ^{4}He baths as well as in vapor and vacuum environments up to 80 K at various biases. We find that the liquid cryogens are unable to mitigate self-heating owing to the thermal boundary resistance between the HEMT surface and the ^{4}He bath. We extract the gate temperature using a small-signal model of the device and show that the trends with the physical temperature are generally consistent with those predicted by a phonon radiation model, regardless of the presence of liquid cryogens. We use these observations to examine the lower bounds of noise performance in cryogenic HEMTs, accounting for the temperature and power dissipation dependence of the thermal noise at the input.

II. EXPERIMENT

A. Overview of measurement apparatus

We measured the microwave noise temperature T_e and gain G of the device under test (DUT), a common-source two-stage packaged amplifier comprising OMMIC D007IH GaAs metamorphic HEMTs,[17] each with a 70 nm gate length and a 4 finger 200 μm width gate structure consisting of an InGaAs–InAlAs–InGaAs–InAlAs epitaxial stack on a semi-insulating GaAs substrate with each stage biased nominally identically, using the cold attenuator Y-factor method.[37] An input matching network (IMN) was employed to match the optimal transistor impedance to the 50 Ω impedance of our measurement system over a 4–5.5 GHz bandwidth (see Sec. S.1 in the supplementary material and Chap. 5.1 of Ref. 38 for more details).

Figure 1(a) shows a schematic of the measurement setup designed for microwave noise characterization in a liquid ^{4}He Dewar. The DUT, a packaged 20 dB chip attenuator, temperature diodes, and heater (mounted behind the stage and not shown) were

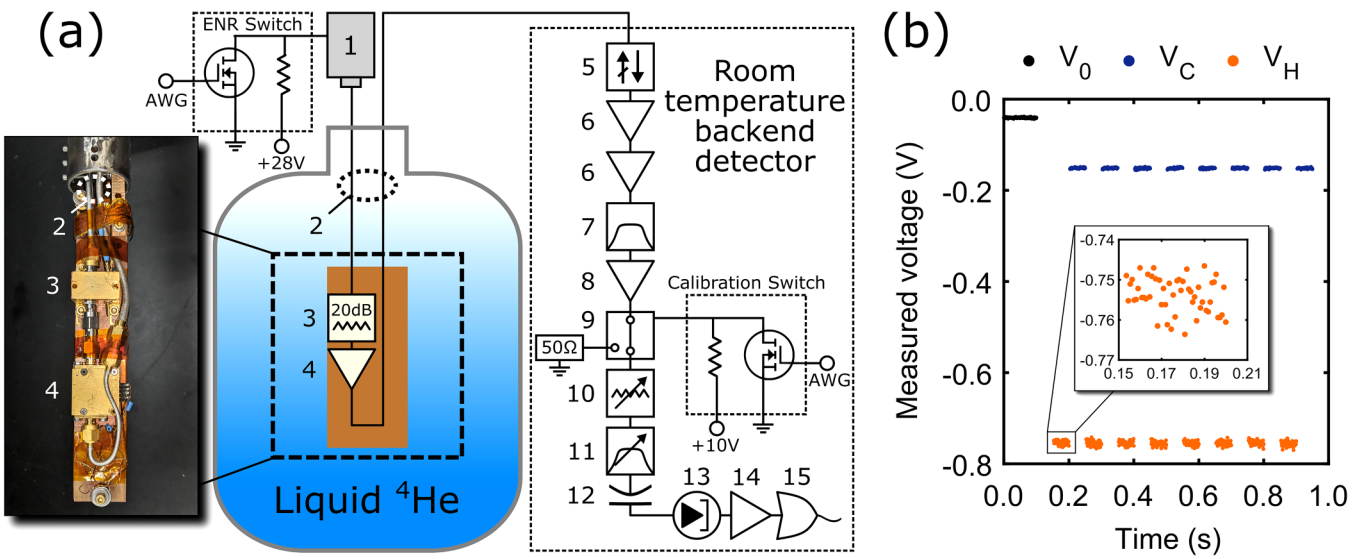

FIG. 1. (a) Schematic of the microwave noise characterization apparatus designed for insertion into a ^{4}He. The image shows the copper mounting stage with the DUT, attenuator, and temperature diodes mounted. A liquid ^{4}He level sensor was mounted behind and above the copper stage inside the dipstick. The components consisted of (1) a 15 dB ENR 2–18 GHz solid state SMA packaged noise diode biased at 28 V through a MOSFET biasing circuit, (2) input and output silver-plated stainless steel SMA coaxial cables each of length 1.3 m, (3) a 20 dB packaged cryogenic chip attenuator with factory calibrated DT-670-SD diodes mounted directly on the attenuator substrate, (4) DUT, (5) a Pasternak PE8327 isolator, (6) Minicircuits ZX60-83LN-S+ low-noise amplifiers, (7) Minicircuits filters with 3–6 GHz bandwidth, (8) a Miteq AMF-3B-04000800-25-25P medium power amplifier, (9) an RF switch for calibration, (10) a 0–20 dB variable attenuator, (11) a Micro Lambda MLFM-42008 20 MHz bandwidth tunable YIG filter, (12) a Pasternak PE8224 inner–outer DC block, (13) a Herotek DT4080 tunnel diode, (14) an SRS560 low-noise preamp, and (15) National Instruments NI6259-USB DAQ. The losses of the SMA cabling and attenuator pads are not shown. (b) Representative raw noise power data vs time. The tunnel diode DC offset voltage V_0 (black symbols), hot voltage V_H (orange symbols), and cold voltage V_C (blue symbols) are all shown. The inset shows a zoom of one V_H pulse.

screw-mounted to a copper mounting stage using indium foil. The stage was screw-mounted to a dipstick, and a liquid level sensor was taped to the interior wall of the dipstick. The dipstick was designed to mount on a 60 L Dewar neck and submerge the stage in the liquid bath. A custom vacuum fitting with hermetic SubMiniature-A (SMA) and DC feedthroughs was sealed to the Dewar neck, allowing for evaporative cooling via pumping. SMA coaxial cables and phosphor-bronze cryogenic wires were used to transmit microwave and DC signals, respectively, between the stage and feedthroughs.

Noise power was generated by a packaged 2–18 GHz solid state SMA noise diode with a 15 dB excess noise ratio (ENR), which was biased using a MOSFET biasing circuit switched by an Agilent 33220A signal generator. This scheme allowed for Y-factor sampling up to 100 kHz, limited by the RC time constant of the MOSFET and the noise diode circuit. Following the cold attenuator method,[39] this noise power was directed through 0.141 in. diameter coaxial cabling to the 20 dB attenuator thermally strapped to the stage. The resulting hot and cold noise temperatures presented to the input plane of the DUT under cryogenic conditions were 52 and 7 K, respectively, yielding a Y-factor of 7.4. The noise power amplified by the DUT was then directed to a room temperature measurement apparatus. The ^{4}He Dewar was earthed, and inner-outer DC blocks were used to connect the hermetic feedthroughs to the noise source and backend to minimize low-frequency bias noise on the DUT.

Figure 1(a) also shows the room temperature backend measurement chain, which consisted of the following components. The microwave power emerging from the SMA feedthrough output first passed through a 3–6 GHz microwave isolator to improve impedance matching and minimize reflections. Two Minicircuits ZX60-83LN-S+ broadband amplifiers were placed sequentially following the isolator. A microwave filter was then used to limit the bandwidth of power amplified by the final gain stage, a Miteq AMF-3B-04000800-25-25P power amplifier. Next, a microwave switch was used to periodically switch between the signal path and a 50 Ω load, enabling re-calibration of the backend to correct for DC offset drifts. A variable attenuator and a temperature-controlled YIG filter were then used to set the magnitude and frequency f of microwave noise power reaching the Herotek DT4080 tunnel diode, which linearly transduced this power into a DC voltage. Inner–outer DC blocks were placed at the tunnel diode's input to eliminate unwanted biasing. The final DC signal was amplified and low-pass filtered by an SRS560 pre-amplifier and then digitized by an analog–digital converter for further data processing.

Figure 1(b) shows representative Y-factor voltage data spanning one duty cycle of data acquisition and backend re-calibration. Here, the hot (noise source on), cold (noise source off), and zero-power offset (50 Ω load) output voltages at time index k, denoted $V_{\mathrm{H},k}$, $V_{\mathrm{C},k}$, and $V_{0,k}$, respectively, were analog filtered at 1 kHz and over-sampled at $f_s = 1.1$ kHz to avoid aliasing artifacts. The noise source was pulsed at $f_{\mathrm{ENR}} = 10$ Hz, and the zero-power offset was re-calibrated at $f_0 = 1$ Hz with a 10% duty cycle, yielding a voltage offset integration time of $t_0 = 0.1 f_0^{-1} = 0.1$ s. Each half-pulse of hot (cold) voltage data was integrated for its duration $t_{\mathrm{ENR}} = 0.5 f_{\mathrm{ENR}}^{-1} = 0.05$ s. The first and last half-pulses of each cycle were discarded due to the 20 ms switching time of the microwave switch, yielding 8 total pulses. The integrated zero-power offset was subtracted from each integrated hot (cold) half-pulse to give hot (cold) offset-corrected data $V'_{\mathrm{H},p}$ ($V'_{\mathrm{C},p}$) for each pulse p. This procedure yielded Y-factor data effectively sampled at f_{ENR} with 0.2 s of data skipped every 1 s. The expression for the measured Y-factor for pulse p considering the above specifications is

$$Y_p = \frac{N_{\mathrm{HC}}^{-1}\left(\sum_{k=k_{\mathrm{H},p}}^{k_{\mathrm{HC},p}} V_{\mathrm{H},k}\right) - N_0^{-1}\left(\sum_{k=1}^{N_0} V_{0,k}\right)}{N_{\mathrm{HC}}^{-1}\left(\sum_{k=k_{\mathrm{HC},p}+1}^{k_{\mathrm{C},p}} V_{\mathrm{C},k}\right) - N_0^{-1}\left(\sum_{k=1}^{N_0} V_{0,k}\right)} = \frac{V'_{\mathrm{H},p}}{V'_{\mathrm{C},p}}, \quad (1)$$

where p ranges from 1 to 8 for each cycle, $N_{\mathrm{HC}} = t_{\mathrm{ENR}} f_s$ is the number of sampled points in each half-pulse, $N_0 = t_0 f_s = 2N_{\mathrm{HC}}$ is the number of sampled points in each calibration pulse, $k_{\mathrm{H},p} = (N_0 + 1) + 2(p-1)N_{\mathrm{HC}}$ is the time index at the start of the pth hot pulse, $k_{\mathrm{HC}} = k_{\mathrm{H},p} + N_{\mathrm{HC}}$ is the time index at the center of the pth pulse when the noise source switches from hot to cold, and $k_{\mathrm{C},p} = k_{\mathrm{H},p} + 2N_{\mathrm{HC}}$ is the time index at the end of the pth cold pulse. For all steady-state data shown in this paper, the Y-factor was further averaged over a total measurement time $t_{\mathrm{fin}} = 4$ s.

A Rhode & Schwarz RSZVA50 VNA calibrated with a Maury 8050CK20 SOLT calibration kit was used for S_{21} measurements. To measure gain and noise temperature simultaneously through Y-factor measurements, the gain $G_{\mathrm{full}} = G L_{\mathrm{coax}}^{-1} L_2^{-1}$ of the entire system from the noise source output plane to the backend input plane was first measured using the VNA, where $L_{\mathrm{coax}} = L_1 L_3$ is the total loss of the cables with input cable loss L_1, output cable loss L_3, and attenuator loss L_2. The DUT gain G could then be extracted from the backend voltage under different conditions using

$$G = G_{\mathrm{full}} L_{\mathrm{coax}} L_2 = \frac{V'_{\mathrm{H}} - V'_{\mathrm{C}}}{V_{\mathrm{H}}^{\mathrm{cal}} - V_{\mathrm{C}}^{\mathrm{cal}}} G_{\mathrm{full}}^{\mathrm{cal}} L_{\mathrm{coax}} L_2, \quad (2)$$

where $V_{\mathrm{H}}^{\mathrm{cal}}$, $V_{\mathrm{C}}^{\mathrm{cal}}$, and $G_{\mathrm{full}}^{\mathrm{cal}}$ are hot and cold output calibration voltages and total calibration gain (including cabling and attenuator), respectively, all measured at a particular device bias. The noise temperature T_e was then determined by

$$T_e = \frac{1}{L_1 L_2}\left[\frac{T_0 E}{Y-1} - T_{\mathrm{C}} - T_{\mathrm{coax}}(L_1 - 1) - T_{L_2}(L_2 - 1)L_1 - \frac{T_{\mathrm{coax}}(L_3 - 1)}{G_{\mathrm{full}} L_3} - \frac{T_{\mathrm{BE}}}{G_{\mathrm{full}}}\right], \quad (3)$$

where $T_0 = 290$ K, E is the noise source excess noise ratio, T_{C} is the noise source physical temperature, T_{coax} is the lumped coaxial cable physical temperature, T_2 is the attenuator physical temperature, and T_{BE} is the backend noise temperature [see Sec. S.2 in the supplementary material for a derivation of Eqs. (2) and (3)].

B. Measurement apparatus calibration

We now describe the calibration procedure for each term of Eqs. (2) and (3). First, the backend noise temperature T_{BE} was independently obtained using a liquid nitrogen cooled fixed load method. The noise source ENR was then calibrated using the backend detector as a reference amplifier (see Sec. S.3 in the

supplementary material for more details). Two separate liquid ^{4}He Dewar baths were then used: one to calibrate the coaxial cable loss and temperature and then the other to calibrate the attenuator loss.

The general procedure in each calibration Dewar was as follows. The dipstick was used to submerge the mounting stage 2 cm from the bottom of a fully filled 60 L liquid ^{4}He Dewar at 4.2 K and ambient pressure. After waiting 30 min for thermal equilibration, calibration measurements were taken. The Dewar was then sealed, and a Leybold DK50 rotary piston vacuum pump was used to evaporatively cool the liquid into the He II phase. An Anest Iwata ISP-500 scroll pump was connected in series and switched on after approximately 2 h of pumping. A steady-state temperature of 1.6 K was reached (corresponding to a vapor pressure of 5.60 Torr) after roughly 6 h of pumping, and further calibration measurements were taken as described in the following paragraphs. A heater was then switched on for less than 2 h to accelerate the boil-off rate of the remaining liquid and switched off when a spike in the stage temperature was observed, which indicated that the liquid surface had dropped below the stage. Further calibration was performed after turning off the heater as the stage was allowed to warm from 1.6 K under the ambient heating power of the measurement apparatus (see Sec. S.3 in the supplementary material for more details). The Dewar was then back-filled with a ^{4}He exchange gas to facilitate thermalization to room temperature, at which point, the dipstick was removed.

We now discuss the details of the measurements in each calibration Dewar. In the first calibration Dewar, the attenuator and DUT shown in the configuration of Fig. 1(a) were replaced with a short through, which was thermally anchored to the copper stage. Figure 2(a) shows the total loss L_{coax} of the coaxial cables measured at room temperature in air and in the first calibration Dewar at 4.2 and 1.6 K. To isolate the individual cable losses L_1 and L_3, these losses were also measured independently at room temperature, and their ratio was assumed to remain constant for all temperatures.

The lumped coaxial cable physical temperature T_{coax}, which is the effective temperature at which the cables radiate their noise power, was measured directly using the Y-factor method. Figure 2(b) shows the measured lumped temperature vs frequency with the cables dipped in a 4.2 K He I bath. We assumed that both cables were at the same physical temperature. The 1.6 K He II calibration measurement is omitted for clarity as it is within 10 K of the He I measurement. To support the accuracy of the measured effective coaxial cable temperature, we estimated the value using an extension of the cable temperature model from Ref. 40. This estimate is shown in Fig. 2(b) and is in agreement with the measured values (see Sec. S.4 in the supplementary material for more details).

In the second calibration Dewar, the short through was replaced by the 20 dB attenuator. The total loss $L = L_{\text{coax}}L_2$ was measured using the same procedure as in the first calibration Dewar, and the attenuator loss L_2 was extracted by dividing L by the previously measured L_{coax}. A measurement of the temperature of the attenuator using the Y-factor method was not possible in this case due to the larger loss of the attenuator. Instead, the temperature T_{L_2} of the attenuator was measured by a calibrated LakeShore DT-670-SD temperature diode indium-bonded directly to the attenuator chip. The diode calibration curve was provided by LakeShore, and the saturated liquid temperature of He I at 4.23 K was used to correct for DC offsets. We assumed that negligible temperature differences existed between the attenuator, mounting stage, and DUT, and we, therefore, took the DUT physical temperature to be $T_{\text{phys}} = T_{L_2}$. All temperature diodes were measured using a LakeShore 336 temperature controller, which converted the temperature to a voltage measured by the DAQ synchronously with all Y-factor measurements.

C. LNA noise and gain measurements

With the calibration data obtained, the noise temperature and gain of the DUT were measured using two additional liquid ^{4}He Dewar baths at various frequencies, temperatures, and biases. The gate-source and drain-source bias voltages V_{GS} and V_{DS}, which were nominally applied equally to each individual transistor, were varied to yield transistor drain–source current densities I_{DS} from 35

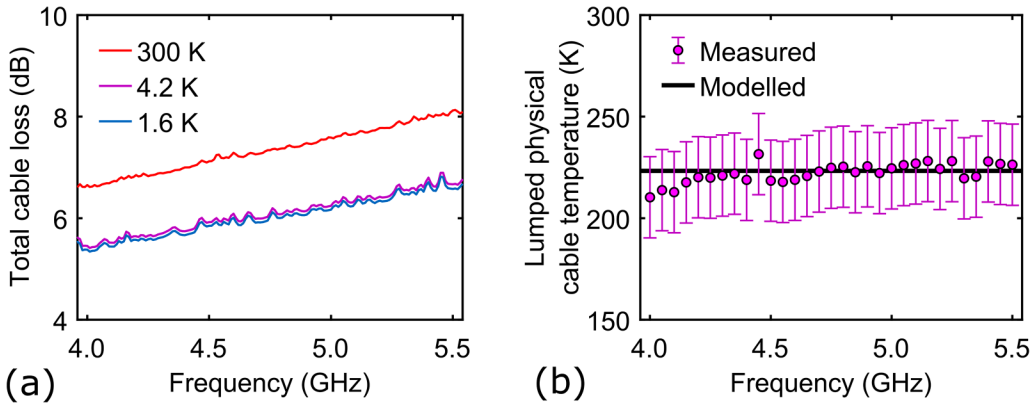

FIG. 2. (a) Total loss of input and output coaxial cables vs frequency measured at 300 (red line), 4.2 (magenta line), and 1.6 K (blue line) with a commercial VNA. (b) Lumped physical coaxial cable temperature vs frequency obtained from Y-factor measurements (magenta circles) and from a heat conduction model (black line). Error bars represent an estimate of the total uncertainty, including systematic errors.

to 120 mA mm^{-1}, corresponding to dissipated power densities P_{DC} per transistor of 15–150 mW mm^{-1}. The relevant measured values from the calibration procedure described above were used to extract G and T_e from Eqs. (2) and (3).

In the first measurement Dewar, the device was mounted to the stage in the configuration shown in Fig. 1(a), and the cooldown procedure followed that of the calibration Dewars described above. At each physical temperature, the DUT bias was varied and Y-factor measurements were taken vs frequency by adjusting the YIG filter frequency. In addition, the calibration measurement of V_H^{cal}, V_C^{cal}, and G_{full}^{cal} was performed, with the DUT bias chosen for convenience to be its low-noise bias. Using these measurements, the device gain G could be extracted from Y-factor voltage measurements at any bias using Eq. (2) without requiring a separate VNA measurement. This calibration was found to be stable over several days, and it was repeated each day before data acquisition.

In addition to measurements under specific liquid cryogen environments, continuous Y-factor measurements were also taken as the He II bath was pumped away, yielding noise data both before and after the DUT gate was submerged. The measurements were performed at a fixed bias of $I_{DS} = 80$ mA mm^{-1} and a frequency of $f = 4.55$ GHz. The bias was chosen to be sufficiently high that any self-heating mitigation would be readily observed without risking device damage due to prolonged biasing, and the frequency was chosen due to it being the optimum noise match frequency as determined by the IMN.[38]

The He II film creep effect[41] was expected to cause the entire mounting stage, including the heated DUT region, to be coated in a superfluid film even after the liquid bath surface dropped below the DUT height. We used the sharp rise observed in the attenuator and stage temperature measurements to indicate the complete evaporation of He II from the stage. The DUT noise was also measured on warming from 1.6 to 80 K in the vacuum space left after all liquid was pumped away. In the second measurement Dewar, the noise temperature was again measured in 4.2 K liquid using the same procedure as in the first measurement Dewar but without the subsequent evaporative cooling step. Instead, the liquid bath was allowed to evaporate under the heating power of the dipstick, enabling measurements to be taken in a vapor environment at several temperatures after the liquid level dropped below the mounting stage. The vapor warmed sufficiently slowly (<1 K/h) such that all measurements were effectively taken in a steady-state vapor environment. The calibrations used for these measurements were the same as for the 4.2 K liquid since the coaxial cable loss and the temperature were observed to change negligibly up to 45 K stage temperature.

III. RESULTS

A. Microwave noise temperature vs frequency

We begin by showing the noise temperature and gain vs frequency at various temperatures, bath conditions, and biases. Figure 3(a) shows T_e and G vs f with the device biased at its low-noise bias of $I_{DS} = 43.9$ mA mm^{-1} and immersed in three different bath conditions ranging from 1.6 K He II to 35.9 K vacuum, with measurements in 4.2 K He I and 8.2 K ^{4}He vapor omitted for clarity since they are within 0.2 K of the He II data. The noise increases monotonically with increasing physical temperature regardless of bath condition. At 4.5 GHz, the noise temperature increases from 2.6 to 3.3 K with the temperature increasing from 20.1 to 35.9 K, consistent with the expected $T_e \propto T_{phys}^{1/2}$ scaling predicted by the Pospieszalski model and observed in prior studies

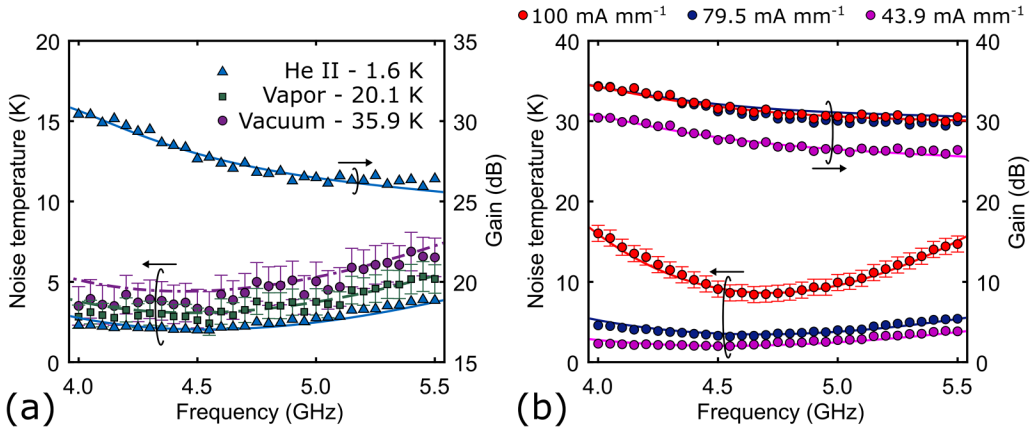

FIG. 3. (a) Noise temperature (left axis) and gain (right axis) vs frequency, measured at the device's low-noise bias of $I_{DS} = 43.9$ mA mm^{-1} ($V_{DS} = 0.56$ V, $P_{DC} = 24.5$ mW mm^{-1}, $V_{GS} = -2.7$ V) in the following cryogenic environments: 1.6 K He II (blue triangles), 20.1 K vapor (green squares), and 35.9 K vacuum (purple circles). Only the gain under He II conditions is shown for clarity since the gain varies by less than 0.5 dB across all temperatures. The small-signal model fits for He II (solid blue line), ^{4}He vapor (dashed green line), and vacuum (dashed–dotted purple line) are also shown. (b) Noise temperature (left axis) and gain (right axis) vs frequency measured at biases of $I_{DS} = 43.9$ mA mm^{-1} (magenta circles; $V_{DS} = 0.56$ V, $P_{DC} = 24.5$ mW mm^{-1}, $V_{GS} = -2.7$ V), $I_{DS} = 79.5$ mA mm^{-1} (dark blue circles; $V_{DS} = 1.0$ V, $P_{DC} = 79.5$ mW mm^{-1}, $V_{GS} = -2.7$ V), and $I_{DS} = 100.0$ mA mm^{-1} (red circles; $V_{DS} = 1.2$ V, $P_{DC} = 120$ mW mm^{-1}, $V_{GS} = -2.7$ V) with the DUT submerged in He II at 1.6 K. To vary the bias, the gate-source voltage was held constant at $V_{GS} = -2.7$ V, while the drain-source voltage V_{DS} was varied. The small-signal model fits (solid lines) are also shown. Where omitted in both (a) and (b), the vertical error bars are equal to the height of the symbols.

[see Fig. 2 from Ref. 42, Fig. 1(c) from Ref. 27, and Fig. 5 from Ref. 43, for example]. The gain varies by approximately 4 dB over the measured frequency range, peaking at $f = 4$ GHz. The gain variation with physical temperature is less than 0.5 dB at fixed f and P_{DC}, and therefore, only the He II gain data are shown for clarity.

Figure 3(b) shows T_e and G vs f with the device immersed in 1.6 K He II at three different device biases of $I_{DS} = 43.9$ mA mm^{-1}, $I_{DS} = 79.5$ mA mm^{-1}, and $I_{DS} = 100.0$ mA mm^{-1}. At biases below $I_{DS} = 79.5$ mA mm^{-1}, the noise temperature varies by less than 1.5 K for all frequencies, whereas the noise temperature increases by 5.3 K from an I_{DS} of 79.5 to 100 mA mm^{-1}. The gain increases monotonically with increasing bias while retaining the same shape vs frequency, but it appears to asymptotically plateau at approximately the highest gain shown here at a bias of $I_{DS} = 100.0$ mA mm^{-1}.

To interpret these measurements, a microwave model of the full device, including IMN, monolithic microwave integrated circuit (MMIC) components, and a transistor small-signal model, was made using Microwave Office.[44] The model used micrograph measured values of the IMN, foundry schematic values for the MMIC, and independently measured small-signal model values from nominally identical discrete transistors from Ref. 45. The small-signal model and IMN parameters were manually tuned by less than 20% from these starting values to fit both the gain and noise temperature curves (see Sec. S.1 in the supplementary material for more details). Representative frequency-dependent results of the model are plotted in Figs. 3(a) and 3(b). The modeled and measured gain are in quantitative agreement over the full frequency range, and the model captures the overall trend in the noise temperature as a function of temperature and bias.

Using this model, we predict the expected change in device noise temperature in different cryogenic environments. Assuming T_g changes from 20 K, the expected elevated gate temperature due to self-heating, to its lowest possible value of 1.6 K, and with all other small-signal parameters remaining unchanged, the model predicts that T_e should decrease from 2.2 to 0.6 K at $f = 4.5$ GHz. As seen in both Figs. 3(a) and 3(b), the lowest measured noise temperature was $T_e = 2.0 \pm 0.2$ K, suggesting a gate temperature closer to 20 K. This initial finding suggests that the liquid cryogens are not altering the self-heating of the gate.

To obtain more quantitative insights, we used the model to extract the gate temperature T_g under various conditions. Figure 4(a) shows the extracted T_g vs T_{phys} at the device's low-noise bias of $I_{DS} = 43.9$ mA mm^{-1}. T_g is elevated above T_{phys} below 20 K even in the presence of superfluid, and equals T_{phys} above 20 K, behavior which is in agreement with prior reports.[26–28] Figure 4(b) shows T_g vs P_{DC} at $T_{phys} = 1.6$ K. Here, T_g changes by less than 2 K for bias powers below ~50 mW mm^{-1} after which T_g increases more rapidly.

We compare the small-signal model results with an equivalent circuit radiation model of the HEMT developed in Ref. 29. The explicit functional form for the gate temperature derived from this model is

$$T_g(T_s, P_{DC}) = \left(T_s^4 + \frac{P_{DC} \mathscr{R}_{cs} \mathscr{R}_{gs}}{\sigma_p (\mathscr{R}_{cs} + \mathscr{R}_{gc} + \mathscr{R}_{gs})} \right)^{1/4}, \quad (4)$$

where T_s is the substrate temperature, $\sigma_p = 850$ W m^{-2} K^{-4} is the equivalent Stefan–Boltzmann constant for phonons in GaAs, and $\mathscr{R}_{ij} = A_i F_{ij}$ is the space resistance between nodes i and j with emitting line length A_i and view factor F_{ij}, which quantifies the fraction of power emitted from surface i that intercepts surface j. The subscripts g, c, and s represent the gate, channel, and substrate, respectively. Following Ref. 30, we take $A_g = A_c = 70$ nm and compute $F_{gc} = 0.3$.

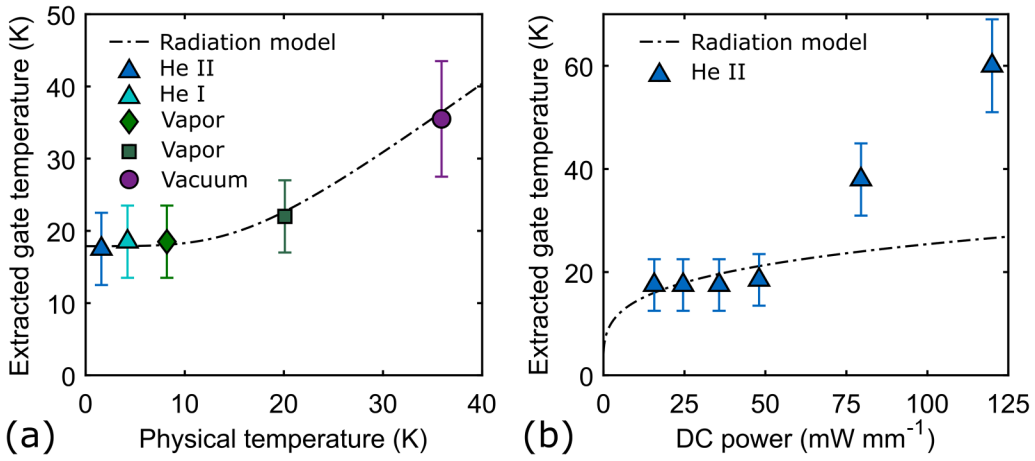

FIG. 4. (a) Extracted gate temperature vs physical temperature at the device's low-noise bias of $I_{DS} = 43.9$ mA mm^{-1} ($V_{DS} = 0.56$ V, $P_{DC} = 24.5$ mW mm^{-1}, $V_{GS} = -2.7$ V). Symbols indicate extracted values and represent the same conditions as in Fig. 3(a), along with extracted values in 4.2 K He I (cyan triangles) and 8.1 K vapor (green diamonds). The radiation model is also shown (dashed–dotted black line). (b) Extracted gate temperature vs bias power at 1.6 K physical temperature (blue triangles). The radiation model is also shown (dashed–dotted black line). In both (a) and (b), the error bars were generated by determining the range of gate temperatures that accounted for the uncertainty in the frequency-dependent noise temperature data.

The predictions of Eq. (4) are also shown in Figs. 4(a) and 4(b). In Fig. 4(a), the data and the radiation model are in quantitative agreement over the full range of physical temperatures. We note that the model contains no fitting parameters. The extracted gate temperatures in the presence of liquid cryogens agree with the radiation model predictions. The increase in the gate temperature with the physical temperature above 20 K at a fixed bias is also captured. In Fig. 4(b), the data and model agree at biases below 50 mW mm^{-1}, but the data deviate from the model above ≈50 mW mm^{-1}. The origin of this discrepancy is presently unclear. A possible explanation is that other noise sources are being attributed to gate thermal noise, leading to artificially high extracted gate temperatures. This additional noise may signal the onset of impact ionization,[46,47] which is associated with a reduction in gain and an increase in gate leakage current. While the gain was observed to plateau at 33 dB at the highest measured bias, as shown in Fig. 3(b), a relatively high gate leakage current of 100 μA was measured, suggesting some contribution of impact ionization. Excluding this non-ideal behavior at high biases, the good agreement in Fig. 4(a) supports the phonon radiation mechanism of heat dissipation in cryogenic HEMTs, and it provides further indication that liquid cryogens provide inadequate cooling power to mitigate self-heating in HEMTs.

B. Noise temperature dependence on cryogenic environment

We obtain further insight into how liquid cryogens impact HEMT noise performance by examining the DUT noise temperature measured continuously in a changing cryogenic environment. Figure 5(a) shows the time series of both T_e and T_{phys} measured continuously as the He II was pumped out of the measurement Dewar. Here, $t = 0$ min was chosen as a reference time at which a rise in T_{phys} was observed, interpreted as the departure of superfluid from the attenuator and device. A corresponding feature in the DUT noise temperature is absent, suggesting that the superfluid cooling has no measurable effect on the DUT noise performance. After $t = 0$ min, the device thermalized with the surrounding ^{4}He vapor, and T_e was observed to increase smoothly with increasing physical temperature. After 20 min, the remaining He II liquid below the stage fully evaporated, and the warming rate increased as the mounting stage and DUT passively warmed to room temperature through the mounting apparatus.

In Fig. 5(b), the warming curve of T_e plotted against T_{phys} is shown from 1.6 to 80 K, taken from the time series in Fig. 5(a). Again, the noise temperature measured in vacuum exhibits no sharp features, instead smoothly varying with physical temperature. Also plotted are noise temperatures measured separately under various bath conditions at the same bias and frequency. The liquid, vapor, and vacuum data all lie within the error bars of the warming curve. These observations suggest that the liquid and vapor cryogen environments provide no self-heating mitigation beyond maintaining a fixed ambient temperature. We note that the high-bias noise temperature exhibits a steeper slope with T_{phys} than expected from the Pospieszalski model and that observed in Fig. 3(a). The origin of the discrepancy may be related to the contribution of impact ionization at this bias, but it does not affect the present discussion, which depends only on the relative difference between noise temperatures in different cryogenic environments.

IV. DISCUSSION

A. Limits on thermal conductance at the ^{4}He-gate interface

We consider our finding that He II is unable to mitigate self-heating in the context of prior studies of He II heat transport properties. We estimate the heat flow $\dot{Q}$ between the He II bath and the HEMT gate surface using $\dot{Q} = hA\Delta T$, where h is the thermal

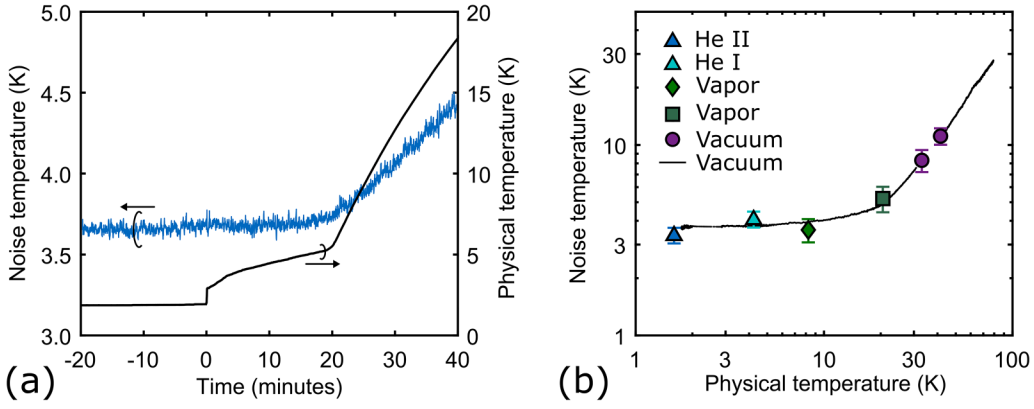

FIG. 5. (a) Noise temperature (left axis, blue line) and physical temperature (right axis, black line) vs time in an evaporating He II bath sampled at $f_{ENR} = 10$ Hz and digitally filtered at 1 Hz, taken at a fixed bias $I_{DS} = 80$ mA mm^{-1} ($V_{DS} = 1.0$ V, $P_{DC} = 80$ mW mm^{-1}, $V_{GS} = -2.8$ V) and frequency $f = 4.55$ GHz. The sharp kink in the physical temperature at time $t = 0$ min is interpreted as the time at which superfluid is no longer present on the attenuator and device and is not reflected in the noise temperature. (b) Noise temperature (black line) vs physical temperature obtained from the transient data shown in (a). Symbols show independently measured noise temperatures representing the same bath conditions as in Fig. 3(a) and the same bias conditions as in (a). The presence of liquid cryogens does not affect the noise temperature within the measurement uncertainty.

boundary conductance, A is the surface area of the gate, and ΔT is the steady-state temperature difference. We note that considerable uncertainty exists in all of these parameters owing to the complex heat transfer regime involving film boiling of superfluid ^{4}He[48] and its dependence on the surface conditions as well as the effective area for heat transfer of the HEMT. We, therefore, expect our estimate to give an order-of-magnitude indication of the heat flux.

To obtain the estimate, we take the surface area to be that of the gate head, $1 \times 200\,\mu\text{m}^2$, which we take as an estimate of the heat transfer area of the dielectric passivation layer, which covers the device. A representative value of the temperature difference if the liquid cryogens measurably decreased the surface temperature is $\Delta T \sim 10$ K. To estimate the heat transfer coefficient, we take $h = 6.2\,\text{kW m}^{-2}\,\text{K}^{-1}$, which is the highest measured He II thermal boundary conductance in the film boiling regime, taken from the compiled data in Table 7.5 from Ref. 32. It is possible that h could exceed this value owing to the micrometer-scale dimensions of the gate per Eq. (7.113) of Ref. 32, but we neglect this effect here.

Assuming a temperature difference $\Delta T = 10$ K, we estimate $\dot{Q} \sim 12\,\mu$W. This value is two orders of magnitude less than the milliwatts of power required to optimally bias the device in our experiment. The absence of any observable effect of cooling by liquid cryogens in our experiment, therefore, indicates that the particular surface conditions of the HEMT do not increase the boiling heat flux sufficiently to make a measurable impact on the microwave noise temperature. This limitation might be mitigated to some by degree by, for instance, increasing the surface area with nanopatterned structures, so long as these structures do not impact noise performance; extensive further investigation would be required to evaluate this strategy.

B. Implications for noise performance of cryogenic HEMTs

We now examine the impact of self-heating on the noise performance of HEMTs assuming that thermal gate noise can only be reduced by decreasing the dissipated DC power. While the gate noise will indeed decrease with less power, the gain will also decrease, leading to an increase in the contribution of both drain noise and any noise source originating after the gain stage of the HEMT, when referred to the input.

We first explore how T_{min} from the Pospieszalski model[20] varies with bias while including the explicit bias dependencies of both T_d and T_g. In the limit $f \ll f_T$, T_{min} is given by[1]

$$T_{\text{min}} = g_0 \frac{\sqrt{T_\text{g} T_\text{d}}}{g_\text{m}}, \tag{5}$$

where we have explicitly introduced the prefactor $g_0 = 4\pi f(C_{\text{gs}} + C_{\text{gd}})\sqrt{(r_i + R_\text{G} + R_\text{S})g_{\text{ds}}}$, which we assume is bias-independent to isolate the bias dependence of Tmin through T_g, T_d, and g_0. We assume $T_{\text{phys}} = 4.2$ K, a gate-source capacitance $C_{\text{gs}} = 150$ fF, a drain-source capacitance $C_{\text{ds}} = 28$ fF, frequency $f = 5$ GHz, a parasitic gate resistance $R_\text{G} = 1\,\Omega$, a parasitic source resistance $R_\text{S} = 1\,\Omega$, an intrinsic input resistance $r_\text{i} = 1\,\Omega$, an intrinsic drain-source conductance $g_{\text{ds}} = 15.4$ mS, and a transconductance g_m obtained by taking a finite-difference approximation of the derivative of $I_{\text{DS}} - V_{\text{DS}}$ data for different V_{GS} separated by 20 mV. All values are taken from Ref. 45. We also assume a drain noise temperature that varies linearly from $T_\text{d} = 20$ K at $I_{\text{DS}} = 0\,\text{mA mm}^{-1}$ to $T_\text{d} = 1000$ K at $I_{\text{DS}} = 100\,\text{mA mm}^{-1}$, an approximation of the bias dependence measured in Ref. 45, while taking $T_\text{d} = 20$ K as the zero-bias limit.

Figure 6(a) shows T_{min} vs dissipated power both with and without the $T_\text{g} \propto P_{\text{DC}}^{1/4}$ dependence predicted by the radiation model. For the case of a fixed gate temperature, we assume $T_\text{g} = 20$ K. The radiation model predicts a lower T_{min} than the fixed T_g model up to a power of $P_{\text{DC}} = 40\,\text{mW mm}^{-1}$ (corresponding to $I_{\text{DS}} = 54\,\text{mA mm}^{-1}$), above which self-heating raises the gate temperature above 20 K. The minimum T_{min} predicted by the

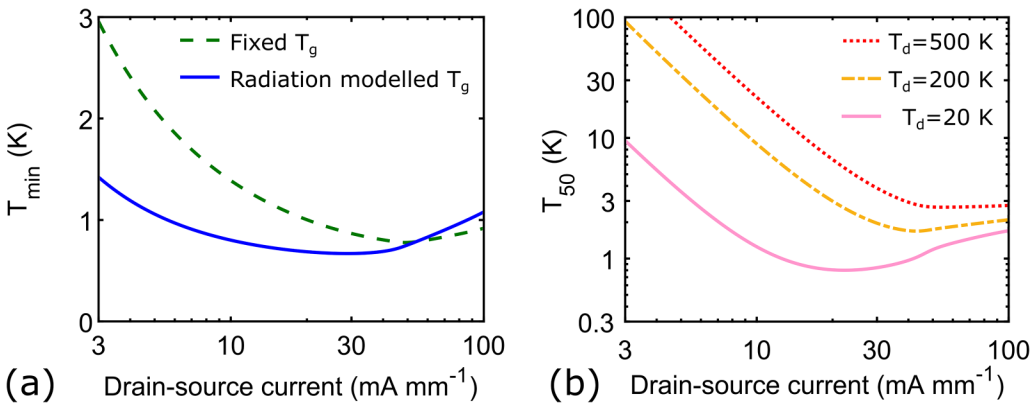

FIG. 6. (a) Modeled T_{min} vs drain-source current, shown for a fixed gate temperature $T_\text{g} = 20$ K (dashed green line) and for a gate temperature with bias dependence determined by a radiation model (solid blue line). The radiation model predicts a gate temperature below 20 K for powers below 40 mW mm^{-1} (corresponding to $I_{\text{DS}} = 54\,\text{mA mm}^{-1}$), which is reflected in T_{min}. (b) Modeled T_{50} noise temperature vs drain-source current, shown for $T_\text{d} = 500$ K (dashed red line), $T_\text{d} = 200$ K (dashed–dotted gold line), and $T_\text{d} = 20$ K (solid pink line). Both the minimum T_{50} and the bias required to achieve this minimum decrease with decreasing T_d.

radiation model is lower than that predicted by the fixed model by 0.12 K, and the bias at which the minimum T_{min} occurs is also lower by 20 mA mm^{-1}. Below this optimal bias, both models predict an increase in T_{min} with decreasing power, indicating where the gain is insufficient to overcome drain noise.

A reduction in drain noise at low biases is evidently beneficial for minimizing noise and power dissipation. We demonstrate the effect such a reduction has on the overall noise temperature using a phenomenological model that both accounts for self-heating and separates the input and output noise contributions additively, a feature of noisy amplifiers, which is not captured in the expression of T_{min}. At low enough frequencies such that $f \ll f_T$, the noise temperature of a HEMT with a 50 Ω source impedance is

$$T_{50} = \frac{T_g(r_i + R_G + R_S) + T_d g_{ds} g_m^{-2}}{50\,\Omega}, \tag{6}$$

as derived in Ref. 38 in the limit of open C_{gs} and C_{gd}. For illustrative purposes, we assume a constant T_d, $T_{phys} = 4.2$ K, and all other parameter values identical to those in the T_{min} model.

Figure 6(b) shows the modeled T_{50} noise temperature vs dissipated power at different drain temperatures. Drain temperatures of 500 K and 200 K were chosen to approximate state-of-the-art low-power performance in GaAs devices[45] and InP devices,[9] respectively. A knee is observed in each curve, the location of which indicates where the gate noise and input-referred drain noise become comparable in magnitude. As T_d is decreased, both the T_{50} value at the knee and the bias at which the knee is observed decrease. This feature is explained as follows: as T_d decreases, less gain is required to achieve the same contribution of T_d to the overall noise, which implies that less power is required to bias the device, ultimately leading to less self-heating and, therefore, a lower T_g. In this way, reducing T_d leads to a simultaneous improvement in noise temperature and reduction in optimal low-noise bias.

V. SUMMARY

We have presented noise measurements of a packaged low-noise GaAs HEMT amplifier immersed in various cryogenic baths. The measured noise temperature and the extracted gate temperature trends are generally consistent with those expected from heat dissipation by phonon radiation, independent of the presence of liquid cryogens. This finding indicates that self-heating of cryogenic GaAs metamorphic HEMTs cannot be mitigated, a result that is expected to extend to cryogenic HEMTs more generally. We explored the consequences of this result on the overall noise performance for various values of the drain temperature. A decreased drain temperature was found to enable simultaneous improvements in noise performance by reducing the necessary gain and hence dissipated power, thereby reducing the self-heating. This result supports the general design principle of cryogenic HEMTs of maximizing gain at the lowest possible power.

SUPPLEMENTARY MATERIAL

See the supplementary material that provides further details on device modeling, a derivation of important equations from the main text, further calibration details, and error analysis.

ACKNOWLEDGMENTS

The authors thank Sander Weinreb, Pekka Kangaslahti, Junjie Li, and Jan Grahn for useful discussions. A.J.A., A.Y.C., B.G., K.A.C., A.C.R., and A.J.M. were supported by the National Science Foundation under Grant No. 1911220. Any opinions, findings, and conclusions or recommendations expressed in this material are those of the authors and do not necessarily reflect the views of the National Science Foundation. J.K. was supported by the Jet Propulsion Laboratory PDRDF under Grant No. 107614-20AW0099. Experimental work was performed at the Cahill Radio Astronomy Laboratory (CRAL) and the Jet Propulsion Laboratory at the California Institute of Technology, under a contract with the National Aeronautics and Space Administration (Grant No. 80NM0018D0004).

AUTHOR DECLARATIONS

Conflict of Interest

The authors have no conflicts to disclose.

Author Contributions

Anthony J. Ardizzi: Conceptualization (equal); Data curation (lead); Formal analysis (lead); Investigation (lead); Methodology (lead); Software (lead); Validation (lead); Visualization (lead); Writing – original draft (lead); Writing – review & editing (equal). **Alexander Y. Choi:** Conceptualization (equal); Investigation (equal); Software (equal). **Bekari Gabritchidze:** Investigation (supporting); Methodology (supporting); Software (supporting); Validation (supporting); Writing – review & editing (supporting). **Jacob Kooi:** Conceptualization (equal); Investigation (equal); Project administration (supporting); Resources (equal); Software (supporting); Supervision (supporting); Validation (supporting); Writing – review & editing (supporting). **Kieran A. Cleary:** Conceptualization (supporting); Funding acquisition (equal); Methodology (supporting); Project administration (supporting); Resources (equal); Supervision (supporting); Validation (supporting); Writing – review & editing (supporting). **Anthony C. Readhead:** Conceptualization (equal); Project administration (supporting); Resources (supporting); Writing – review & editing (supporting). **Austin J. Minnich:** Conceptualization (equal); Funding acquisition (lead); Methodology (equal); Project administration (equal); Resources (equal); Supervision (equal); Validation (equal); Writing – original draft (supporting); Writing – review & editing (equal).

DATA AVAILABILITY

The data that support the findings of this study are available from the corresponding author upon reasonable request.

REFERENCES

[1]M. Pospieszalski, IEEE Microw. Mag. **6**, 62 (2005).
[2]J. J. Bautista, "HEMT low-noise amplifiers," in *Low-Noise Systems in the Deep Space Network*, Deep-Space Communications and Navigation Series, edited by M. S. Reid (Wiley, Hoboken, NJ, 2008), Chap. 5, pp. 195–254.

[3]M. W. Pospieszalski, "Extremely low-noise cryogenic amplifiers for radio astronomy: Past, present and future," in *2018 22nd International Microwave and Radar Conference (MIKON)* (IEEE, 2018), pp. 1–6.
[4]C.-C. Chiong, Y. Wang, K.-C. Chang, and H. Wang, IEEE Microw. Mag. **23**, 31 (2022).
[5]J. Bautista *et al.*, "Cryogenic, X-band and Ka-band InP HEMT based LNAs for the deep space network," in *2001 IEEE Aerospace Conference Proceedings (Cat. No. 01TH8542)* (IEEE, 2001), Vol. 2, pp. 2/829–2/842.
[6]J. M. Chow, J. M. Gambetta, E. Magesan, D. W. Abraham, A. W. Cross, B. R. Johnson, N. A. Masluk, C. A. Ryan, J. A. Smolin, S. J. Srinivasan, and M. Steffen, Nat. Commun. **5**, 4015 (2014).
[7]J. M. Hornibrook *et al.*, Phys. Rev. Appl. **3**, 024010 (2015).
[8]P. Krantz *et al.*, Appl. Phys. Rev. **6**, 021318 (2019).
[9]E. Cha *et al.*, "A 300-μW cryogenic HEMT LNA for quantum computing," in *2020 IEEE/MTT-S International Microwave Symposium (IMS)* (IEEE, 2020), pp. 1299–1302, ISSN: 2576–7216.
[10]J. C. Bardin, D. H. Slichter, and D. J. Reilly, IEEE J. Microw. **1**, 403 (2021).
[11]N. Wadefalk, A. Mellberg, I. Angelov, M. E. Barsky, S. Bui, E. Choumas, R. W. Grundbacher, E. L. Kollberg, R. Lai, N. Rorsman, P. Starski, J. Stenarson, D. C. Streit, and H. Zirath, IEEE Trans. Microw. Theory Tech. **51**, 1705 (2003).
[12]J. Schleeh, G. Alestig, J. Halonen, A. Malmros, B. Nilsson, P. A. Nilsson, J. P. Starski, N. Wadefalk, H. Zirath, and J. Grahn, IEEE Electron Device Lett. **33**, 664 (2012).
[13]A. H. Akgiray, S. Weinreb, R. Leblanc, M. Renvoise, P. Frijlink, R. Lai, and S. Sarkozy, IEEE Trans. Microw. Theory Tech. **61**, 3285 (2013).
[14]M. Varonen *et al.*, "A 75–116-GHz LNA with 23-K noise temperature at 108 GHz," in *2013 IEEE MTT-S International Microwave Symposium Digest (MTT)* (IEEE, 2013), pp. 1–3, ISSN: 0149-645X.
[15]D. Cuadrado-Calle, D. George, G. A. Fuller, K. Cleary, L. Samoska, P. Kangaslahti, J. W. Kooi, M. Soria, M. Varonen, R. Lai, and X. Mei, IEEE Trans. Microw. Theory Tech. **65**, 1589 (2017).
[16]E. Cha *et al.*, IEEE Trans. Microw. Theory Tech. **66**, 4860 (2018).
[17]F. Heinz, F. Thome, A. Leuther, and O. Ambacher, "Noise performance of sub-100-nm metamorphic HEMT technologies," in *2020 IEEE/MTT-S International Microwave Symposium (IMS)* (IEEE, 2020), pp. 293–296, ISSN: 2576–7216.
[18]E. Cha, "InP high electron mobility transistors for cryogenic low noise and low power amplifiers," Ph.D thesis (Chalmers University of Technology, Göteborg, 2020), ISBN: 9789179054076.
[19]J. Schleeh, "Cryogenic ultra-low noise inP high electron mobility transistors," Ph.D thesis (Chalmers University of Technology, Göteborg, 2013).
[20]M. W. Pospieszalski, IEEE Trans. Microw. Theory Tech. **37**, 1340 (1989).
[21]H. Statz, H. Haus, and R. Pucel, IEEE Trans. Electron Devices **21**, 549 (1974).
[22]M. W. Pospieszalski, "On the limits of noise performance of field effect transistors," in *2017 IEEE MTT-S International Microwave Symposium (IMS)* (IEEE, 2017), pp. 1953–1956.
[23]T. Gonzalez, O. M. Bulashenko, J. Mateos, D. Pardo, L. Reggiani, and J. M. Rubí, Semicond. Sci. Technol. **12**, 1053 (1997).
[24]I. Esho, A. Y. Choi, and A. J. Minnich, J. Appl. Phys. **131**, 085111 (2022).
[25]J. J. Bautista and E. M. Long, Interplanet. Netw. Progr. Rep. **42–170**, 1 (2007).
[26]K. H. G. Duh, W. F. Kopp, P. Ho, P.-C. Chao, M.-Y. Ko, P. M. Smith, J. M. Ballingall, J. J. Bautista, and G. G. Ortiz, IEEE Trans. Electron Devices **36**, 1528 (1989).
[27]J. Schleeh, J. Mateos, I. de-la-Torre, N. Wadefalk, P. A. Nilsson, J. Grahn, and A. J. Minnich, Nat. Mater. **14**, 187 (2015).
[28]M. A. McCulloch, J. Grahn, S. J. Melhuish, P.-A. Nilsson, L. Piccirillo, J. Schleeh, and N. Wadefalk, J. Astron. Telesc. Instrum. Syst. **3**, 014003 (2017).
[29]A. Y. Choi, I. Esho, B. Gabritchidze, J. Kooi, and A. J. Minnich, J. Appl. Phys. **130**, 155107 (2021).
[30]A. Y. Choi, "Investigation of electronic fluctuations in semiconductor materials and devices through first-principles simulations and experiments in transistor amplifiers," Ph.D thesis (California Institute of Technology, 2022).
[31]J. T. Muhonen, M. Meschke, and J. P. Pekola, Rep. Prog. Phys. **75**, 046501 (2012).
[32]S. W. Van Sciver, *Helium Cryogenics* (Springer, New York, 2012).
[33]S. W. Van Sciver, "Applications of superfluid helium in large-scale superconducting systems," in *Quantized Vortex Dynamics and Superfluid Turbulence*, edited by R. Beig *et al.* (Springer, Berlin, 2001), Vol. 571, pp. 51–65.
[34]P. Lebrun, L. Serio, L. Tavian, and R. Weelderen, "Cooling strings of superconducting devices below 2 K: The helium II bayonet heat exchanger," in *Advances in Cryogenic Engineering*, edited by P. Kittel (Springer US, Boston, MA, 1998), pp. 419–426.
[35]B. Baudouy, in *Proceedings of the CAS-CERN Accelerator School: Superconductivity for Accelerators* (CERN, 2014).
[36]P. Lebrun, "Twenty-three kilometres of superfluid helium cryostats for the superconducting magnets of the large hadron collider (LHC)," in *Cryostat Design*, edited by J. Weisend II (Springer International Publishing, Cham, 2016), pp. 67–94.
[37]M. Leffel and R. Daniel, "The Y factor technique for noise figure measurements," Rohde & Schwarz Technical Application Note No. IMA178, version 5e (2021), https://scdn.rohde-schwarz.com/ur/pws/dl_downloads/dl_application/application_notes/1ma178/1MA178_5e_NoiseFigure.pdf.
[38]A. H. Akgiray, "New technologies driving decade-bandwidth radio astronomy: Quad-ridged flared horn and compound-semiconductor LNAs," Ph.D thesis (California Institute of Technology, 2013).
[39]J. E. Fernandez, Telecommun. Mission Oper. Progr. Rep. **135**, 1 (1998).
[40]A. Soliman, A. Janzen, and S. Weinreb, "Thermal modelling of coaxial line for cryogenic noise measurements," in *2016 URSI Asia-Pacific Radio Science Conference (URSI AP-RASC)* (IEEE, Seoul, 2016), pp. 900–903.
[41]J. F. Allen and A. Misener, Proc. R. Soc. London, Ser. A **172**, 467 (1939).
[42]M. Pospieszalski *et al.*, "Very low noise and low power operation of cryogenic AlInAs/GaInAs/InP HFET's," in *1994 IEEE MTT-S International Microwave Symposium Digest (Cat. No. 94CH3389-4)* (IEEE, San Diego, CA, 1994), pp. 1345–1346.
[43]M. W. Pospieszalski, "On the dependence of FET noise model parameters on ambient temperature," in *2017 IEEE Radio and Wireless Symposium (RWS)* (IEEE, Phoenix, AZ, 2017), pp. 159–161.
[44]AWR Microwave Office; see https://www.cadence.com/en_US/home/tools/system-analysis/rf-microwave-design/awr-microwave-office.html.
[45]B. Gabritchidze *et al.*, "Experimental characterization of temperature-dependent microwave noise of discrete HEMTs: Drain noise and real-space transfer," in *2022 IEEE/MTT-S International Microwave Symposium (IMS)* (IEEE, 2022).
[46]M. Somerville, A. Ernst, and J. del Alamo, IEEE Trans. Electron Devices **47**, 922 (2000).
[47]R. Webster, S. Wu, and A. Anwar, IEEE Electron Device Lett. **21**, 193 (2000).
[48]D. Labuntzov and Y. Ametistov, Cryogenics **19**, 401 (1979).